

## Tuning Bifunctional Properties of $\alpha$ -Fe<sub>2</sub>O<sub>3</sub>/Fe<sub>2</sub>TiO<sub>5</sub>/Pt Heterojunction Photoelectrode for Light-Induced Water Oxidation and Oxygen Reduction Activity

Hasmat Khan<sup>a,b</sup>, Alireza Razazzadeh<sup>a</sup>, Mehdi Shamekhi<sup>c,d</sup>, Gilles H. Peslherbe<sup>c,d,e</sup>, Myung-Jin Jung<sup>a</sup>, Susanta Bera<sup>f</sup>, and Se-Hun Kwon<sup>a,b\*</sup>

<sup>a</sup>School of Materials Science and Engineering, Pusan National University, Busan 46241, Republic of Korea

<sup>b</sup>Institute of Materials Technology, Pusan National University, Busan 46241, Republic of Korea

<sup>c</sup>Department of Physics, Concordia University, Montreal, QC H4B 1R6, Canada

<sup>d</sup>Centre for Research in Molecular Modeling, Concordia University, Montreal, QC H4B 1R6, Canada

<sup>e</sup>Department of Chemistry and Biochemistry, Concordia University, Montreal, QC H4B 1R6, Canada

<sup>f</sup>Dutch Institute for Fundamental Energy Research (DIFFER), 5612AJ Eindhoven, The Netherlands

\*Correspondence: [sehun@pusan.ac.kr](mailto:sehun@pusan.ac.kr) (S.-H. Kwon)

Keywords: Alpha hematite, Bifunctional heterojunction photoelectrode, Pt nanoparticles, Atomic layer deposition, Solar rechargeable zinc-air battery

## Contents

Calculation for capacity, energy density, and power density of the battery.....	S-3
DFT calculation.....	S-3
<b>Fig. S1:</b> SEM studies of as-prepared and heat-treated samples .....	S-4
<b>Fig. S2:</b> LSV study of FT samples with different ALD-TiO <sub>2</sub> cycles.....	S-4
<b>Fig. S3:</b> SEM-EDS studies of the FT samples with different ALD-TiO <sub>2</sub> cycles.....	S-5
<b>Fig. S4:</b> High-resolution SEM images of the F, FT, and FTPt samples.....	S-6
<b>Fig. S5:</b> TEM studies of the FTPt sample.....	S-7
<b>Fig. S6:</b> High-resolution TEM image of FTPt and Pt nanoparticles distribution curve....	S-7
<b>Fig. S7:</b> High-resolution TEM analysis of the FTPt sample with 50 ALD-Pt cycles.....	S-8
<b>Fig. S8:</b> XPS survey spectra of the FTPt sample.....	S-8
<b>Fig. S9:</b> Photoelectrochemical studies of the photoelectrodes.....	S-9
<b>Fig. S10:</b> Light induced-ORR and WOR performance of the photoelectrodes.....	S-9
<b>Fig. S11:</b> Light induced-ORR performance of the FTPt photoelectrode .....	S-10
<b>Fig. S12:</b> Nyquist plots of the FTPt photoelectrode at different potentials.....	S-10
<b>Fig. S13:</b> XPS studies of the FTPt photoelectrode after ORR performance.....	S-11
<b>Fig. S14:</b> Data obtained from computational investigations.....	S-12
<b>Fig. S15:</b> Galvanostatic charging and discharging curves of the SRZB.....	S-13
<b>Fig. S16:</b> TEM studies of the FTPt sample after the battery cycling stability.....	S-13
<b>Fig. S17:</b> Battery charging-discharging cycles using commercial Pt/C catalyst.....	S-14
<b>Fig. S18:</b> Linear polarization curve of the SRZB under light and dark conditions.....	S-14
<b>Table S1:</b> Photocurrent densities of FT samples with different ALD-TiO <sub>2</sub> cycles.....	S-15
<b>Table S2:</b> Onset potentials of WOR and ORR for the F, FT, and FTPt samples.....	S-15
<b>Table S3:</b> EIS curves fitting data.....	S-15
<b>Table S4:</b> R <sub>p</sub> values of FTPt sample at various ORR-relevant potentials.....	S-15
<b>Table S5:</b> E <sub>fb</sub> and N <sub>d</sub> values obtained from M-S plot.....	S-16
<b>Table S6:</b> Comparison table for recently developed cathode materials.....	S-16
<b>Reference.....</b>	S-17

Calculation for specific capacity, energy density, and power density of the Zn–air battery using the following equations (1–3):

$$\begin{aligned}\text{Specific Capacity (mAh/cm}^2) &= (I \times t)/A \\ &= (0.1 \times 50)/1 \\ &= 5 \text{ mAh/cm}^2\end{aligned}\quad (1)$$

where,  $I$ = discharge current (mA),  $t$ = discharge time (h), and  $A$ = electrode area ( $\text{cm}^2$ ).

$$\begin{aligned}\text{Power density (mW/cm}^2) &= (V \times I)/A \\ &= (1.1 \times 0.1)/1 \\ &= 0.11 \text{ mW/cm}^2\end{aligned}\quad (2)$$

where,  $V$ = discharge voltage (V),  $I$ = current (mA), and  $A$ = electrode area ( $\text{cm}^2$ ).

$$\begin{aligned}\text{Energy density} &= V \times \text{Capacity (mAh/cm}^2) \\ &= (1.1 \times 5) \\ &= 5.5 \text{ mWh/cm}^2\end{aligned}\quad (3)$$

### DFT calculation:

Spin-polarized density functional theory (DFT) calculations were performed using the GPAW code based on the projector-augmented wave (PAW) method within the generalized gradient approximation (GGA-PBE). A plane-wave cut-off energy of 500 eV and a Monkhorst–Pack k-point grid of  $9 \times 5 \times 5$  were used for the orthorhombic  $\text{Fe}_2\text{TiO}_5$  unit cell (space group Pbcn, 32 atoms). To address band gap underestimation, the DFT+U approach was applied with  $U = 4.3$  eV for Fe 3d orbitals [1-3]. The  $\text{Fe}_2\text{TiO}_5$ -Pt heterostructure was modelled using a three-layered (101)  $\text{Fe}_2\text{TiO}_5$  slab and a two-layered  $2 \times 2$  Pt (111) surface, with a 20 Å vacuum in the z-direction. Structural optimization was performed until atomic forces were below 0.05 eV/Å [1-3].

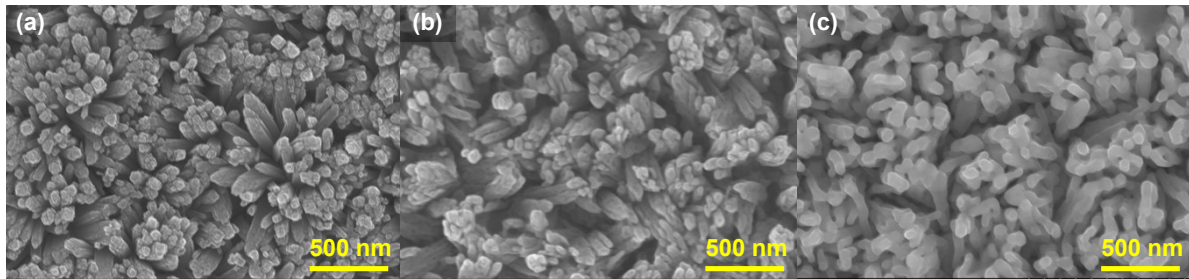


**Fig. S1:** (a) Top-view SEM image of FeOOH nanorod arrays, (b)  $\alpha$ - $\text{Fe}_2\text{O}_3$  nanorod arrays cured at 550 °C, and (c)  $\alpha$ - $\text{Fe}_2\text{O}_3$  nanorod arrays cured at 750 °C.

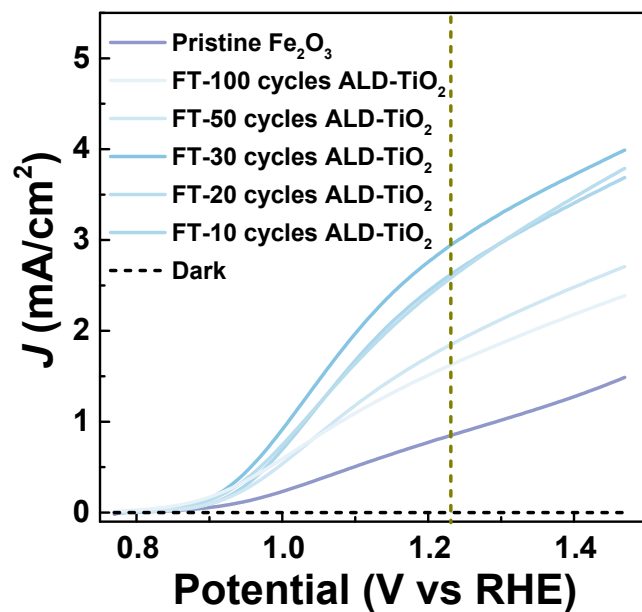


**Fig. S2:** Linear sweep voltammetry curves of the FT samples with different  $\text{Fe}_2\text{TiO}_5$  shell thicknesses varied by changing ALD- $\text{TiO}_2$  cycles from 10 to 100.

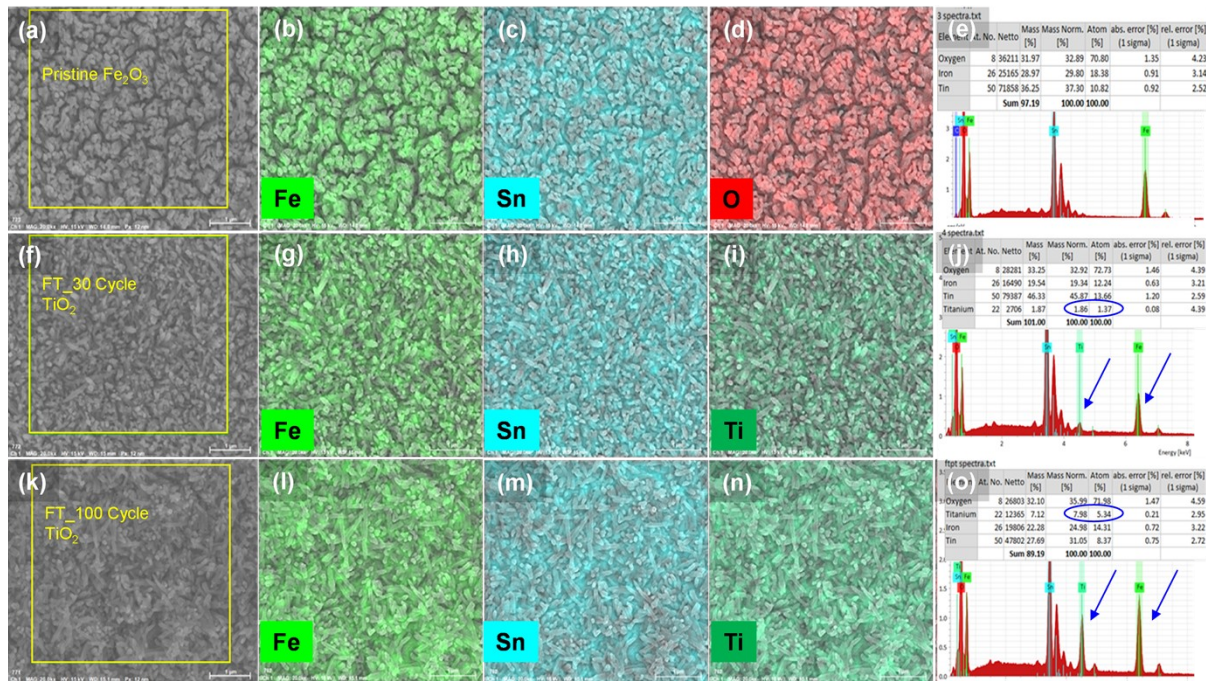


**Fig. S3:** SEM-EDS studies of the FT samples with different ALD-TiO<sub>2</sub> cycles; (a) top-view SEM image of the pristine  $\alpha$ -Fe<sub>2</sub>O<sub>3</sub> nanorod arrays, (b–d) are the EDS elemental mapping images for Fe, Sn, and O elements, respectively taken from the yellow marked area in (a), (e) EDS shows the elemental composition of the pristine  $\alpha$ -Fe<sub>2</sub>O<sub>3</sub> sample, (f) top-view SEM image of the FT sample with 30 cycles ALD-TiO<sub>2</sub>, (g–i) are the EDS elemental mapping images for Fe, Sn, and Ti elements, respectively taken from the yellow marked area in (f), (j) EDS shows the elemental composition of the FT sample with 30 cycles ALD-TiO<sub>2</sub>, (k) the SEM image of the FT sample with 100 cycles ALD-TiO<sub>2</sub>, (l–n) are the EDS elemental mapping images for Fe, Sn, and Ti elements, respectively taken from the yellow marked area in (k), and (o) EDS shows the elemental composition of the FT sample with 100 cycles ALD-TiO<sub>2</sub>.

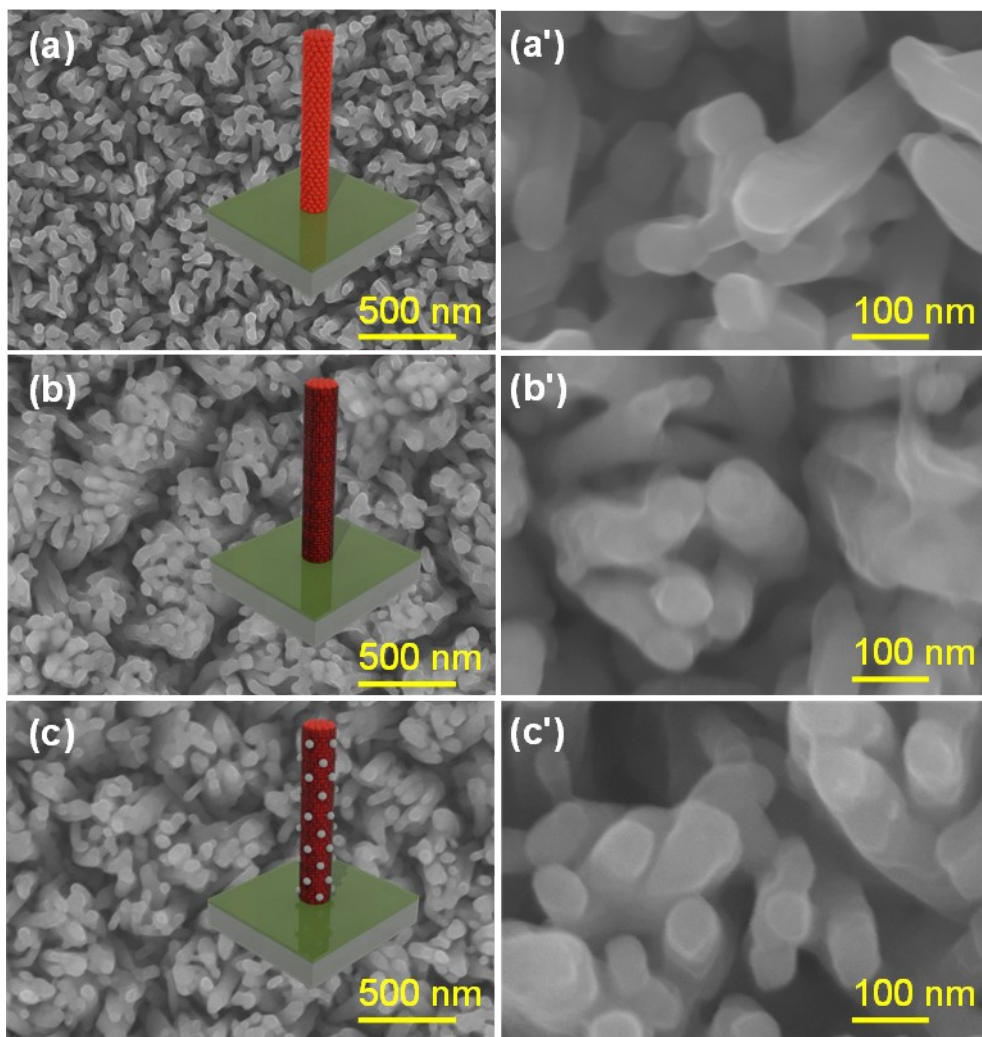


**Fig. S4:** Top-view SEM images of the F, FT, and FTPt samples grown on FTO substrate; (a,a') different magnified SEM images of F sample, (b,b') different magnified SEM images of FT sample, and (c,c') different magnified SEM images of FTPt sample. Insets of (a–c) are the schematic drawing of the respective nanostructured photoelectrodes.

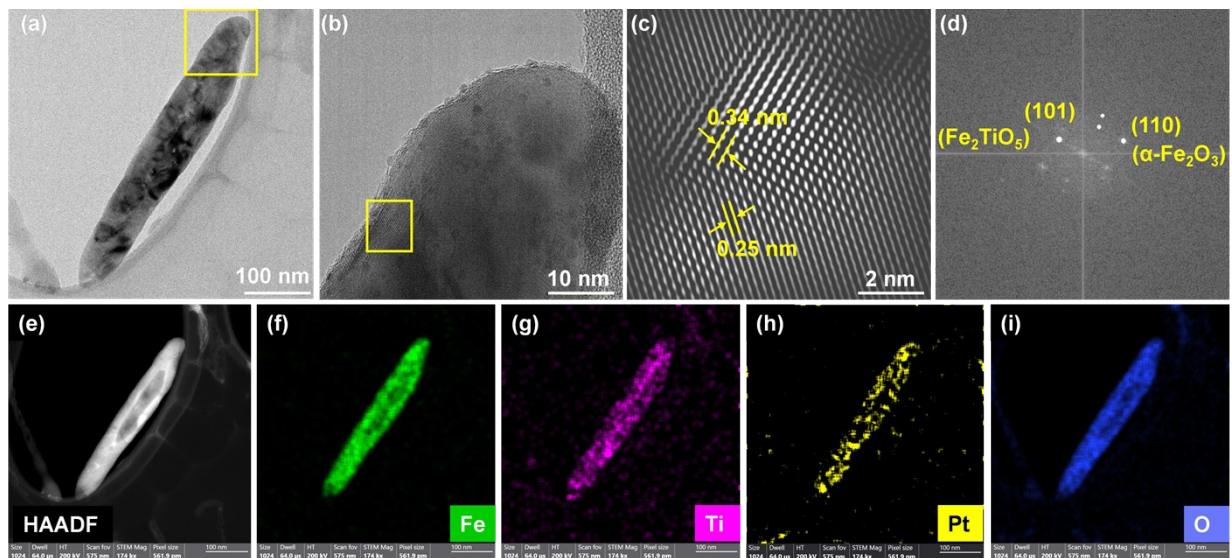


**Fig. S5:** TEM studies of the FTPt sample; (a) low-magnification TEM image, (b) HRTEM image taken from the yellow marked area in (a), (c,d) HRTEM image shows the lattice fringes and their corresponding FFT images, taken from the yellow marked area in (b), (e) HAADF image, and (f–i) corresponding EDS elemental-mapping images confirm the presence of Fe, Ti, Pt, and O elements.

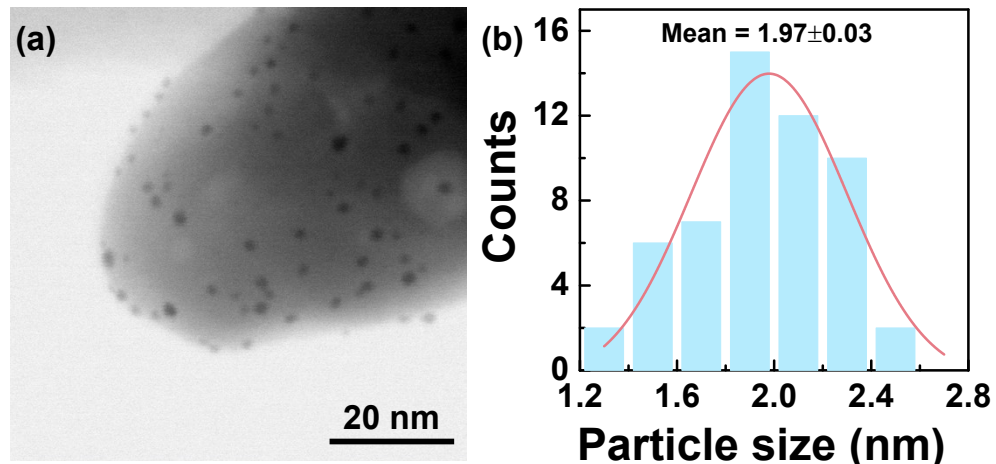


**Fig. S6:** (a) TEM image of FTPt sample and (b) particle size distribution curve Pt nanoparticles.

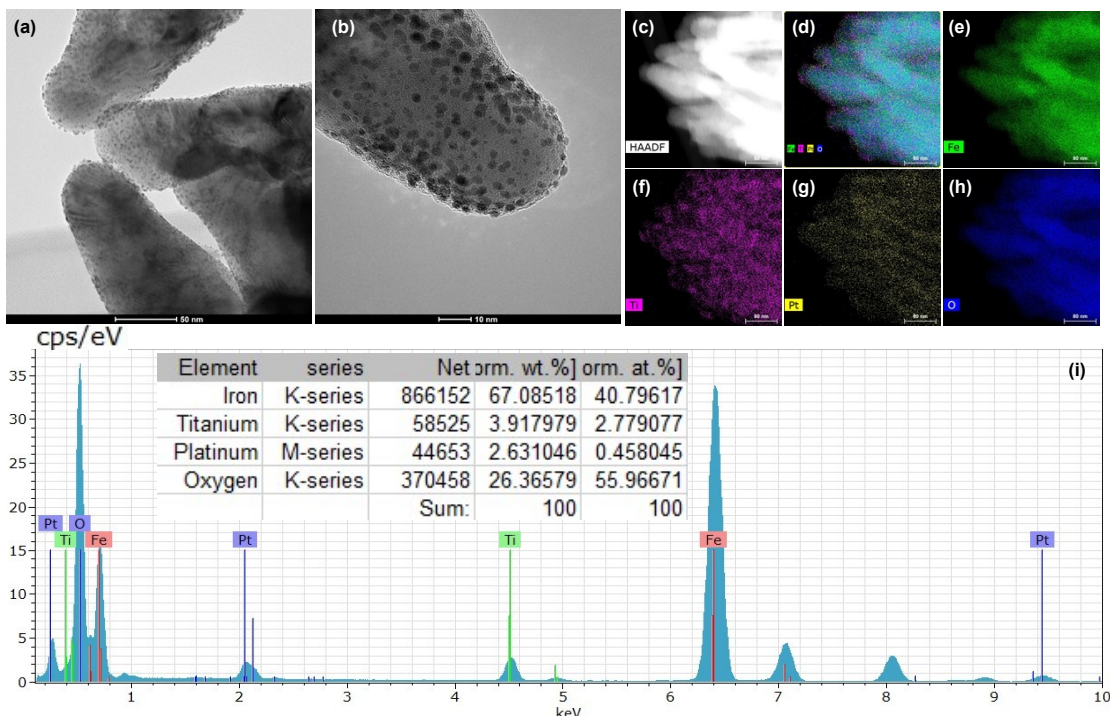


**Fig. S7:** TEM analysis of the FTPt sample with 50 ALD-Pt cycles: (a,b) Bright-field TEM images showing Pt nanoparticles decorated on the  $\alpha$ -Fe<sub>2</sub>O<sub>3</sub>/Fe<sub>2</sub>TiO<sub>5</sub> nanorod; (c) HAADF image; (d-h) corresponding EDS elemental mapping confirming the presence of Fe, Ti, Pt, and O; (i) TEM-EDS spectra with quantitative elemental composition (inset).

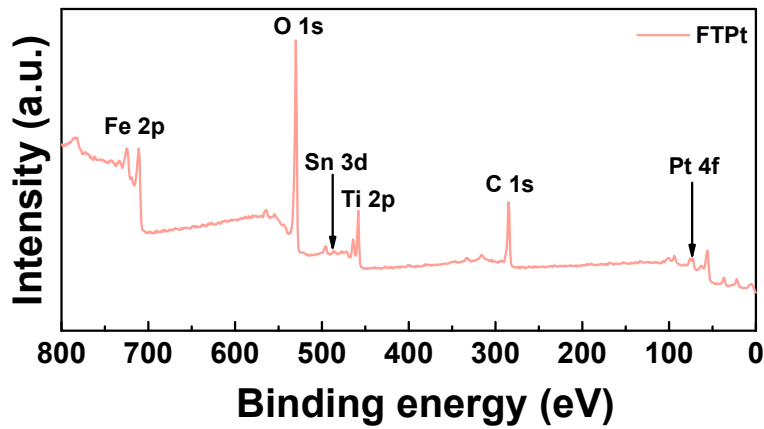


**Fig. S8:** XPS survey spectra of the FTPt sample.

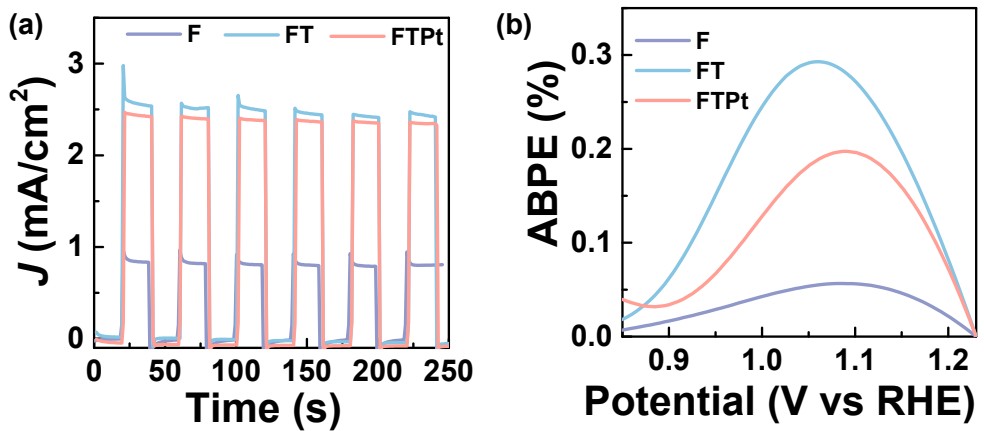


**Fig. S9:** (a) The transient chronoamperometric ( $J$ - $t$ ) curves measured under the chopped light illumination, and (b) applied bias photon to current efficiencies (ABPE) of all the photoelectrodes.

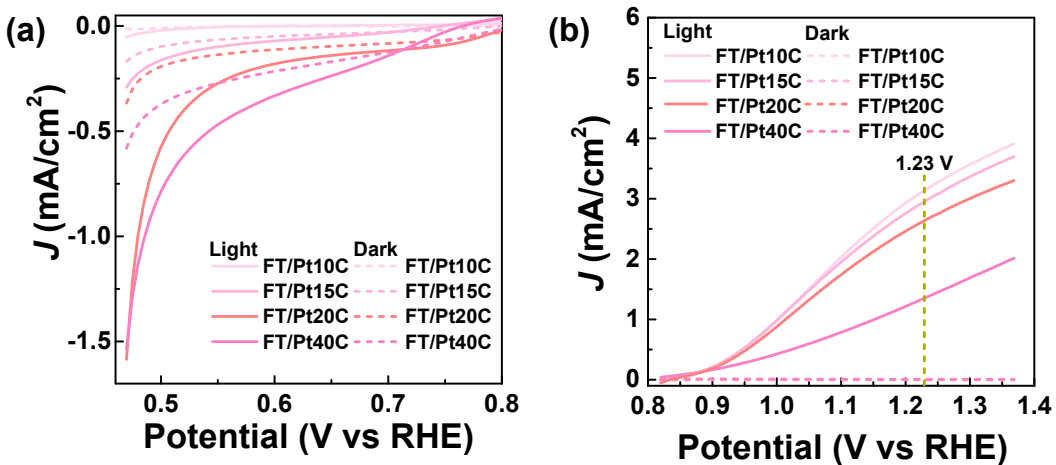


**Fig. S10:** Light induced-ORR and WOR performance of the photoelectrodes; (a) LSV curves for ORR photocurrent, and (b) LSV curves for WOR photocurrent.

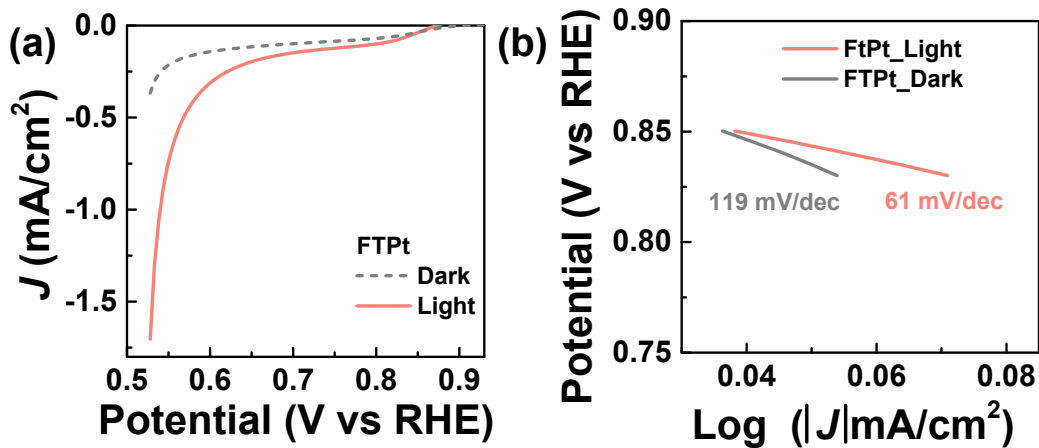


**Fig. S11:** Light induced-ORR performances of the FTPt photoelectrode under light and dark conditions: (a) LSV curves and (b) Tafel slope.

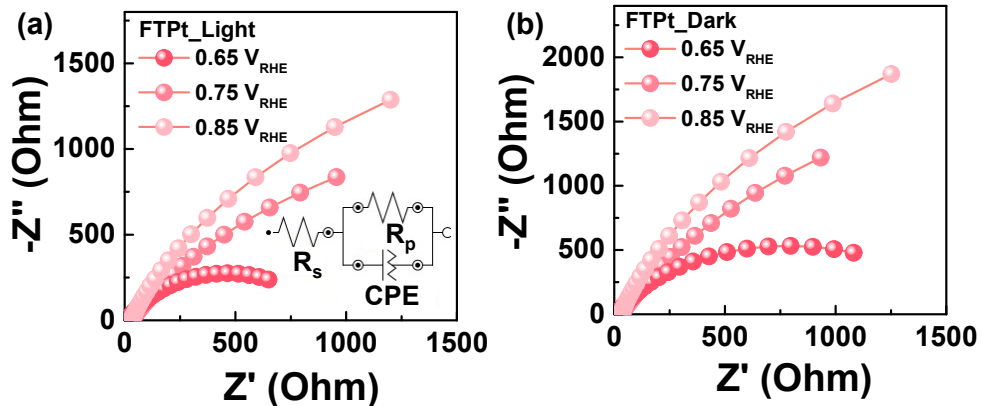


**Fig. S12:** Nyquist plots of the FTPt photoelectrode measured at various ORR-relevant potentials in 1 M KOH aqueous electrolyte under (a) light and (b) dark conditions. Inset of (a) shows the equivalent circuit model used for fitting.

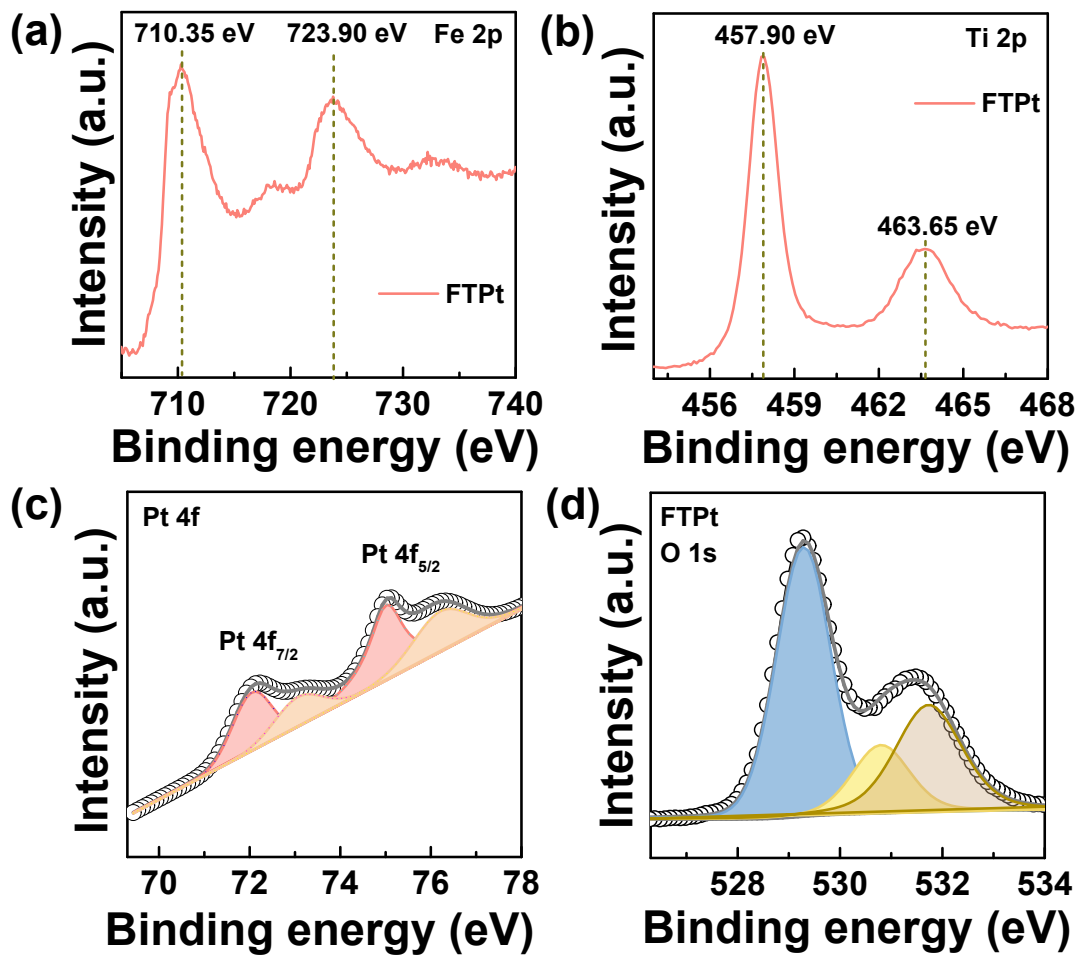


**Fig. S13:** XPS studies of the FTPt photoelectrode after ORR performance test: (a,b) the high-resolution spectra of Fe 2p and Ti 2p; (c,d) are the XPS spectra for Pt 4f and O 1s.

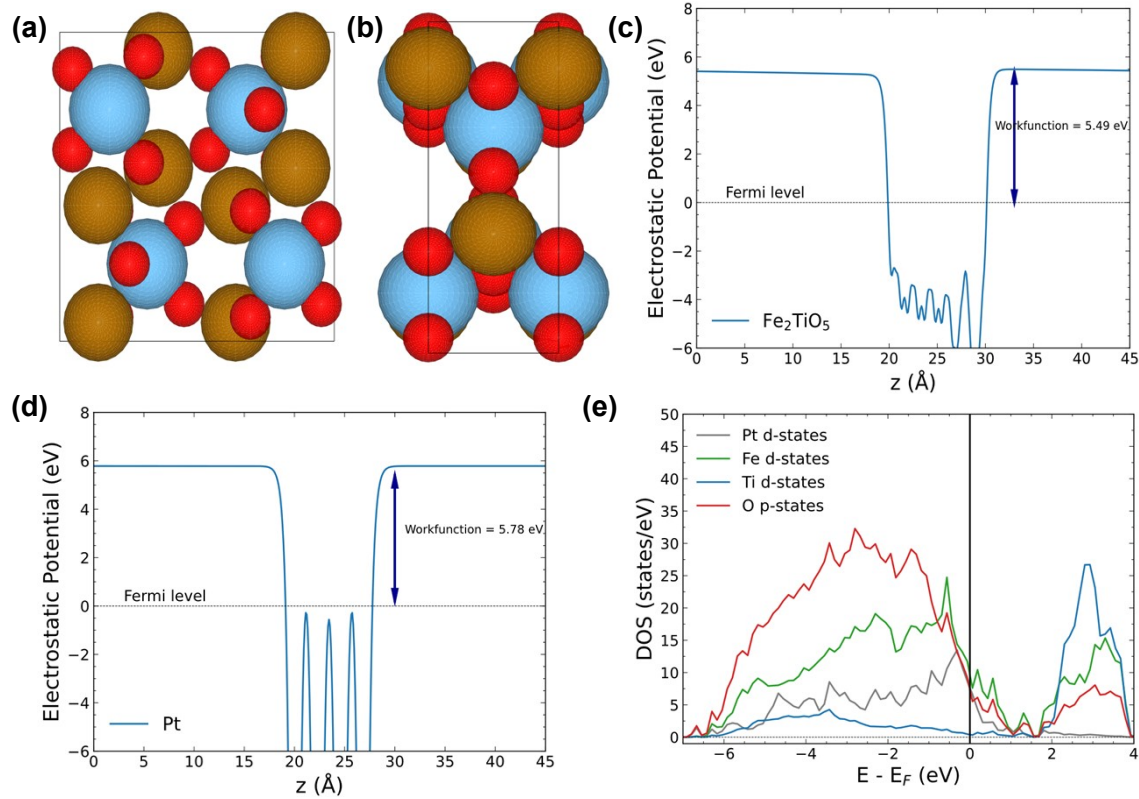


**Fig. S14:** The orthorhombic unit cell of  $\text{Fe}_2\text{TiO}_5$  with 63 space group (32 atoms): (a) side and (b) top view of  $\text{Fe}_2\text{TiO}_5$ . Atom colors: Fe (brown), Ti (blue) and O (red). The average electrostatic potential for (c)  $\text{Fe}_2\text{TiO}_5$  and (d) Pt along the  $z$ -axis. (e) Represents the DOS of  $\text{Fe}_2\text{TiO}_5/\text{Pt}$  heterojunction projected into d-states of Fe, Ti and p-states of O.

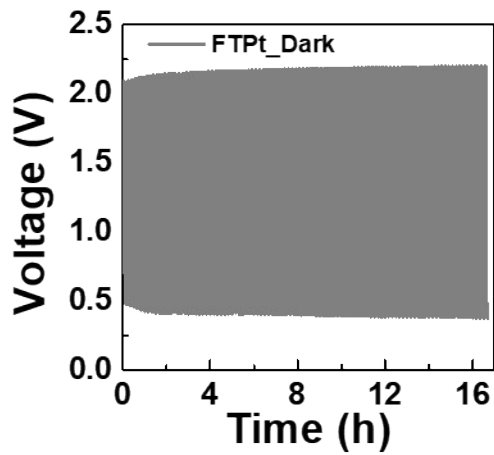


**Fig. S15:** The galvanostatic charging and discharging curves of the SRZB in dark condition with the FTPt photoelectrode as cathode at a current density of  $0.5 \text{ mA/cm}^2$ .

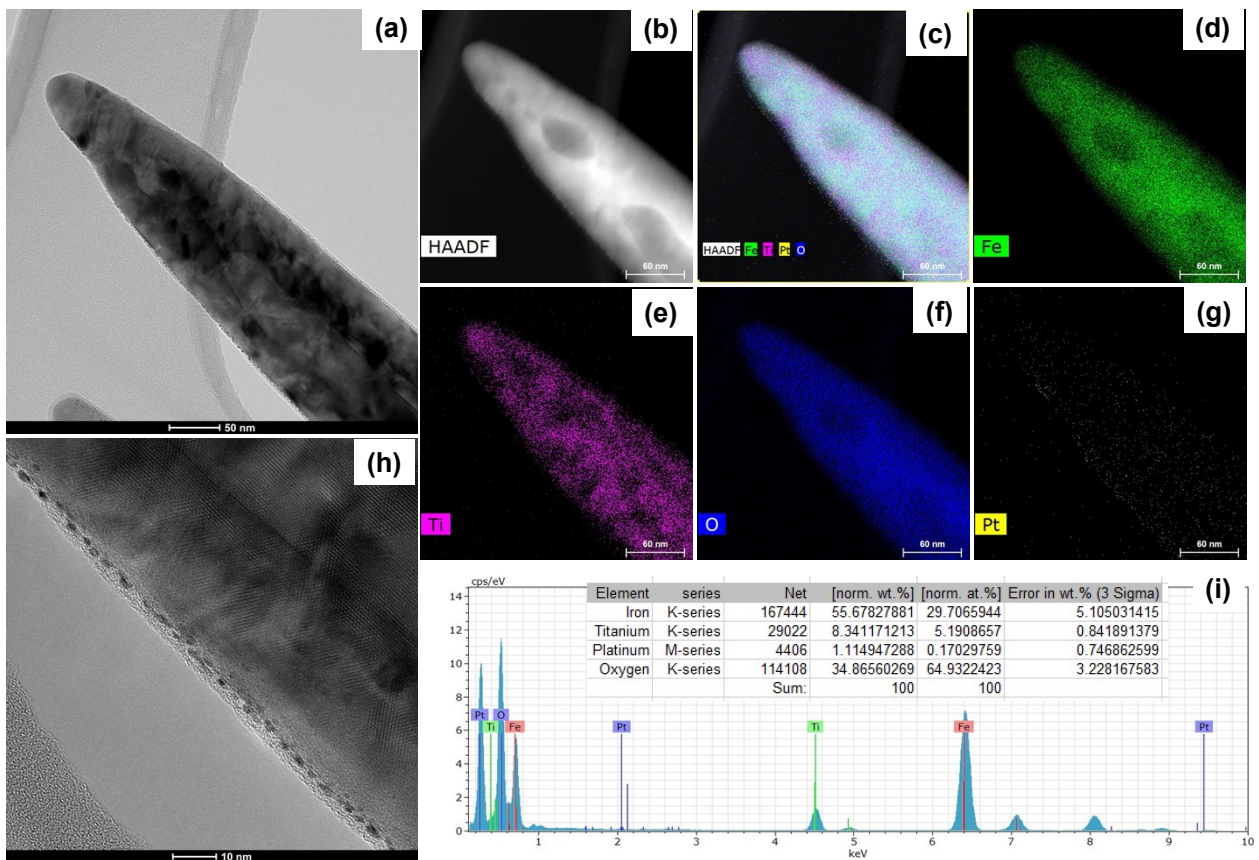


**Fig. S16:** TEM studies of the FTPt sample after the galvanostatic charging and discharging cycling test; (a) bright field TEM image, (b) HAADF image, (c–g) EDS elemental-mapping images of Fe,

Ti, O, and Pt elements, respectively, (h) high magnified TEM bright field image, and (i) quantitative TEM-EDS confirms the presence of Fe, Ti, Pt, and O elements.

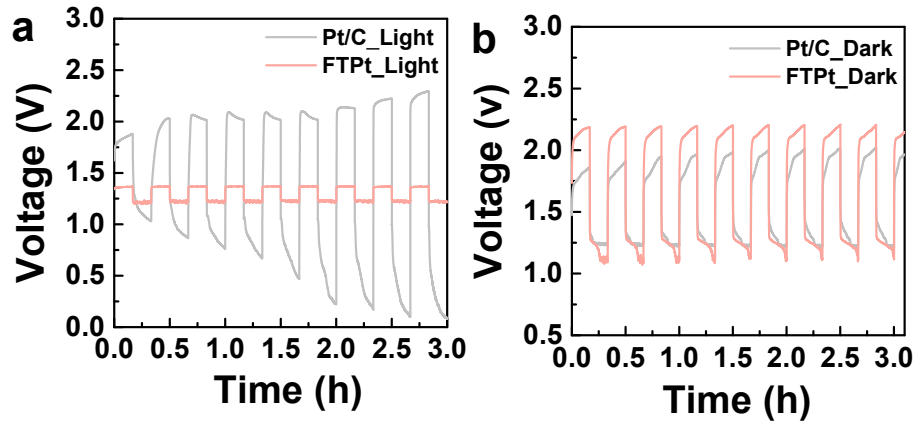


**Fig. S17:** Charging-discharging cycles using a commercial Pt/C catalyst under identical conditions for comparison purposes: (a) the charging/discharging cyclic stability test of Pt/C and FTPt samples under light illumination and (b) Pt/C and FTPt samples under dark condition.

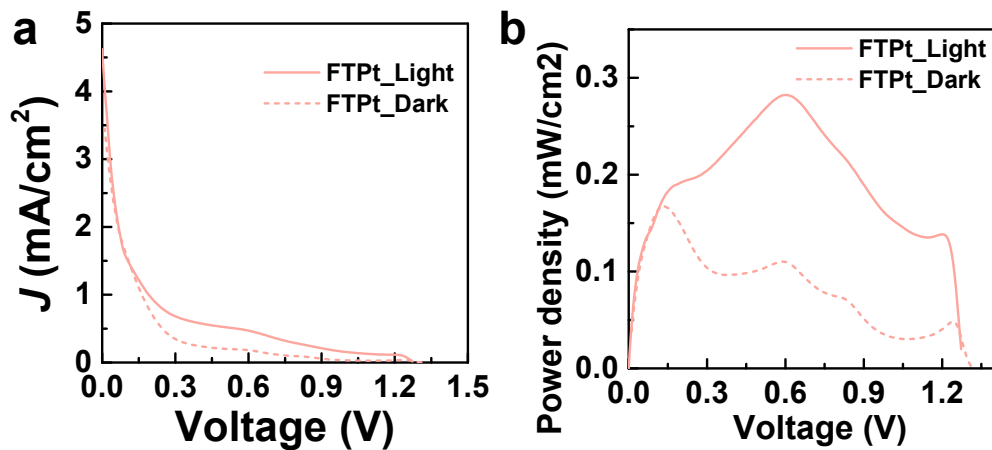


**Fig. S18:** (a) Linear polarization curve of the SRZB under light and dark conditions and (b) estimated power density curve obtained from the corresponding polarization data.

**Table S1:** Photocurrent densities of FT samples with different ALD-TiO<sub>2</sub> cycles.

Samples	Photocurrent at 1.23 V vs. RHE
Pristine Fe <sub>2</sub> O <sub>3</sub>	0.86 mA/cm <sup>2</sup>
FT-100 cycle ALD-TiO <sub>2</sub>	1.62 mA/cm <sup>2</sup>
FT-50 cycle ALD-TiO <sub>2</sub>	1.85 mA/cm <sup>2</sup>
FT-30 cycle ALD-TiO <sub>2</sub>	2.94 mA/cm <sup>2</sup>
FT-20 cycle ALD-TiO <sub>2</sub>	2.62 mA/cm <sup>2</sup>
FT-10 cycle ALD-TiO <sub>2</sub>	2.57 mA/cm <sup>2</sup>

**Table S2:** Light-induced WOR and ORR onset potentials of the F, FT, and FTPt samples.

Sample	WOR onset potential (V vs RHE)	ORR onset potential (V vs RHE)
F	0.90	---
FT	0.87	0.47
FTPt	0.90	0.80

**Table S3:** Charge transfer resistance (R<sub>p</sub>), solution resistance (R<sub>s</sub>), and capacitance (CPE) values of the F, FT, and FTPt samples under dark and light conditions were obtained by fitting the EIS curves to an equivalent circuit to the impedance data.

Sample	R <sub>p</sub> (Ω)		R <sub>s</sub> (Ω)		CPE (Ω <sup>-1</sup> )	
	Dark	Light	Dark	Light	Dark	Light
F	41352	3823	24.9	20.3	7.6×10 <sup>-6</sup>	3.1×10 <sup>-5</sup>
FT	2183	325	28.0	27.0	5.3×10 <sup>-5</sup>	9.0×10 <sup>-5</sup>
FTPt	2894	547	20.0	19.0	4.0×10 <sup>-5</sup>	5.0×10 <sup>-5</sup>

**Table S4:** The R<sub>p</sub> values of FTPt sample at various ORR-relevant potentials under dark and light conditions were obtained by fitting the EIS curves to an equivalent circuit to the impedance data.

FTPt	R <sub>p</sub> -Light	R <sub>p</sub> -Dark
0.65 V <sub>RHE</sub>	895 (Ω)	1.54 (KΩ)
0.75 V <sub>RHE</sub>	4.95 (KΩ)	5.71 (KΩ)
0.85 V <sub>RHE</sub>	6.63 (KΩ)	6.71 (KΩ)

**Table S5:** The calculated values of  $E_{fb}$  and  $N_d$  from the M-S plot measured under light illumination.

Photoelectrodes	Flat band potential ( $E_{fb}$ )	Charge carriers' concentration ( $N_d$ )
F	0.29 V vs RHE	$3.81 \times 10^{19} \text{ cm}^{-3}$
FT	0.12 V vs RHE	$4.71 \times 10^{21} \text{ cm}^{-3}$
FTPt	0.12 V vs RHE	$4.18 \times 10^{21} \text{ cm}^{-3}$

**Table S6:** Comparison table for recently developed cathode materials of the same types for solar rechargeable Zn-Air batteries.

Cathode	Current (mA/cm <sup>2</sup> )	Charging potential (V)	Discharging potential (V)	Stability	Light source	Ref.
$\alpha\text{-Fe}_2\text{O}_3/\text{Fe}_2\text{TiO}_5/\text{Pt}$	0.1	1.4	1.15	50 h	100 mW/cm <sup>2</sup>	This work
W:BiVO <sub>4</sub> /V <sub>2</sub> O <sub>5</sub>	0.3	1.0	2.0	4 h	100 mW/cm <sup>2</sup>	[4]
CdS/TiO <sub>2</sub>	0.5	2.8	0.5	6 h	-----	[5]
ZnO/CuO	0.1	1.5	1.28	22 h	100 mW/cm <sup>2</sup>	[6]
PDTB and TiO <sub>2</sub>	0.1, 5.0	0.59, 0.86	1.90, 1.18	22 h	90 mW/cm <sup>2</sup>	[7]
pTTh	0.1	1.98	1.78	64 h	300 W Xe-lamp	[8]
$\alpha\text{-Fe}_2\text{O}_3$	0.5	1.64	1.15	50 h	500 W Xe-lamp	[9]
PEDOT-PEO-CNTs-PUF	0.2	1.66	1.15	-----	300 mW/cm <sup>2</sup>	[10]
NCO-HNF	2	1.9	1.2	26 h	100 mW/cm <sup>2</sup>	[11]
Ni <sub>12</sub> P <sub>5</sub> @NCNT	1	1.98	0.98	-----	300 W Xe-lamp	[12]
g-C <sub>3</sub> N <sub>4</sub> /CuZIF-	2	2.0	1.14	333 h	150 W Xe-lamp	[13]
67						

## Reference

- [1] Mortensen, Jens Jørgen, et al. "GPAW: An open Python package for electronic structure calculations." *The Journal of Chemical Physics* 160.9 (2024).
- [2] Larsen, Ask Hjorth, et al. "The Atomic Simulation Environment—A Python library for working with atoms" *J. Phys.: Condens. Matter* 29 (2017).
- [3] Perdew, John P., Kieron Burke, and Matthias Ernzerhof. "Generalized gradient approximation made simple." *Physical review letters* 77.18 (1996): 3865.
- [4] T. S. Andrade, I. C. Sena, L. C. A. de Oliveira, P. Lianos, M. C. Pereira, *Mater. Today Commun.*, 2021, **28**, 102546.
- [5] T. S. Andrade, M. C. Pereira, P. Lianos, *J. Electroanal. Chem.*, 2020, **878**, 114559.
- [6] D. Bu, M. Batmunkh, Y. Zhang, Y. Li, B. Qian, Y. Lan, X. Hou, S. Li, B. Jia, X. M. Song, T. Ma, *Chem. Eng. J.*, 2022, **433**, 133559.
- [7] D. Du, S. Zhao, Z. Zhu, F. Li, J. Chen, *Angew. Chem. Int. Ed. Engl.* 2020, **59**, 18140–18144.
- [8] D. Zhu, Q. Zhao, G. Fan, S. Zhao, L. Wang, F. Li, J. Chen, *Angew. Chem. Int. Ed. Engl.*, 2019, **58**, 12460–12464.
- [9] X. Liu, Y. Yuan, J. Liu, B. Liu, X. Chen, J. Ding, X. Han, Y. Deng, C. Zhong, W. Hu, *Nat. Comm.*, 2019, **10**, 4767.
- [10] Z. Fang, Y. Zhang, X. Hu, X. Fu, L. Dai, D. Yu, *Angew. Chem. Int. Ed.* 2019, **58**, 9248–9253.
  
- [11] C. Tomon, S. Sarawutanukul, N. Phattharasupakun, S. Duangdangchote, P. Chomkhundtod, P. Kidkhunthod, M. Sawangphruk, *Electrochim. Acta.*, 2021, **392**, 139022.
- [12] J. Lv, S. C. Abbas, Y. Huang, Q. Liu, M. Wu, Y. Wang, L. Dai, *Nano Energy*, 2018, **43**, 130–137.
- [13] R. Ren, G. Liu, J. Y. Kim, R. E. A. Ardhi, M. X. Tran, W. Yang, J. K. Lee, *Appl. Catal. B: Environ.*, 2022, **306**, 121096.